

Robust and Safe Multi-Agent Reinforcement Learning Framework with Communication for Autonomous Vehicles

Keshawn Smith

Department of ECE
University of Connecticut
keshawn.smith@uconn.edu

Zhili Zhang

School of Computing
University of Connecticut
zhili.zhang@uconn.edu

H M Sabbir Ahmad

Department of ECE
Boston University
sabbir92@bu.edu

Ehsan Sabouni

Department of ECE
Boston University
esabouni@bu.edu

Maniak Mondal

School of Computing
University of Connecticut
mainak.mondal@uconn.edu

Song Han

School of Computing
University of Connecticut
song.han@uconn.edu

Wenchao Li

Department of ECE
Boston University
wenchao@bu.edu

Fei Miao

School of Computing
University of Connecticut
fei.miao@uconn.edu

Abstract: Deep multi-agent reinforcement learning (MARL) has been demonstrated effectively in simulations for many multi-robot problems. For autonomous vehicles, the development of vehicle-to-vehicle (V2V) communication technologies provide opportunities to further enhance safety of the system. However, zero-shot transfer of simulator-trained MARL policies to hardware dynamic systems remains challenging, and how to leverage communication and shared information for MARL has limited demonstrations on hardware. This problem is challenged by discrepancies between simulated and physical states, system state and model uncertainties, practical shared information design, and the need for safety guarantees in both simulation and hardware. This paper introduces RSR-RSMARL, a novel Robust and Safe MARL framework that supports Real-Sim-Real (RSR) policy adaptation for multi-agent systems with communication among agents, with both simulation and hardware demonstrations. RSR-RSMARL leverages state (includes shared state information among agents) and action representations considering real system complexities for MARL formulation. The MARL policy is trained with robust MARL algorithm to enable zero-shot transfer to hardware considering the sim-to-real gap. A safety shield module using Control Barrier Functions (CBFs) provides safety guarantee for each individual agent. Experiment results on F1/10th-scale autonomous vehicles with V2V communication demonstrate the ability of RSR-RSMARL framework to enhance driving safety and coordination across multiple configurations. These findings emphasize the importance of jointly designing robust policy representations and modular safety architectures to enable scalable, generalizable RSR transfer in multi-agent autonomy.

Keywords: Robust Multi-Agent Reinforcement Learning, Safe Multi-Agent Reinforcement Learning, MARL with Communication

1 Introduction

The U.S. Department of Transportation (USDOT) has recently outlined a national plan to introduce Vehicle-to-Everything (V2X) technologies to roadways, aiming to reduce traffic-related fatalities and injuries [1]. As the potential benefits of Connected and Autonomous Vehicles (CAVs) continue to gain recognition, there has been an increase in research exploring their capabilities and

applications [2, 3, 4]. Multi-Agent Reinforcement Learning (MARL) has shown great promise in autonomous vehicle research, particularly in learning optimal decision-making strategies in dynamic environments [2, 5, 6, 7, 8]. MARL-based decision-making strategies for CAVs promise to enhance road safety, reduce traffic congestion, and improve transportation efficiency, and the benefits can be further improved with communication between vehicles and surrounding infrastructure. However, despite these advances, there is currently no open-source testbed designed to support MARL methodology validations considering the above mentioned functions, existing testbed either lack open-source code or some components to validate the full stack design [9, 3, 10, 11]. This gap in available resources significantly limits the ability to develop and test MARL-based decision-making algorithms in realistic, CAV-specific contexts.

Deep reinforcement learning in robots has garnered significant attention [11]. However, sim-to-real transfer still presents substantial challenges, primarily due to the discrepancies between simulated and actual environments. It is challenging to simulate the rich real-world complexities such as noise, uncertainties, scenarios, etc. These discrepancies can lead to performance degradation when policies trained in simulation are deployed in real-world scenarios, and methods like domain randomization [12, 13] significantly increases training computational cost. Moreover, ensuring safety is critical for multi-agent systems. CAVs operate in dynamic environments where interactions with other vehicles and human operators are frequent, and unsafe actions could lead to catastrophic failures. For CAVs, state or model uncertainties, sensor inaccuracies, and communication delays must be properly managed to ensure the robustness, safety, and effectiveness of the learned policies under real-world conditions. Hence, it is crucial to incorporate mechanisms that guarantee safety during both learning and deployment to real-world system phases under uncertainties.

In this work, we propose a novel **Real-Sim-Real** Multi-Agent Reinforcement Learning (RSR-MARL) framework to address the critical challenge of minimizing the sim-to-real gap, by aligning the design of our MARL problem formulation and policy training algorithm with the intended real-world environment where they will be deployed. To enhance system safety, we incorporate a Control Barrier Function (CBF)-based *Safety Shield*. The high level planning such as keeping lane or changing lane is calculated by robust MARL algorithm [14, 15], while low level safe controller is calculated through the safety shield. The safety shield dynamically adjusts the set of safe actions for each agent, ensuring adherence to predefined safety constraints throughout the training and testing process. Meanwhile, the integration of the *Safety Shield* is a flexible and modular design, which can be seamlessly adapted to different simulation or testbed dynamical systems by using the corresponding controller (such as MPC with the physical dynamic model of the testbed), while the overall training process remains fundamentally unchanged. Additionally, our framework integrates communication delays directly into the training loop, effectively simulating shared observation delays between an ego vehicle and its neighboring vehicles in the environment. By incorporating these real-world constraints into the training process, our framework ensures that the learned policies are robust and zero-shot transferrable to the hardware. The key contributions of this work are as follows: (1) We introduce **RSR-RSMARL**, a robust and safe MARL framework with communication among agents to evaluate multi-agent systems such CAVs in **Real-Sim-Real** settings. It addresses challenges such as state and model uncertainties, communication delays, and safety in multi-agent real-world environments. (2) We perform experiments in both the CARLA simulator and real-world settings. In the simulator, we train the MARL algorithm in an idealized environment and evaluate its performance using key metrics, including safety and efficiency. (3) To the best of our knowledge, we provide the first hardware demonstration of robust and safe MARL with communication for multi-agent systems such CAVs. The real-world experiments on 1/10th-scale autonomous vehicles demonstrate the simulation-trained policy’s performance under various scenarios including ablation studies. Through these experiments, we evaluate the agents’ ability to navigate real-world environments while ensuring safe and adaptive behavior.

The results of our study highlight the effectiveness of the **RSR-RSMARL** pipeline in safely and successfully transferring MARL policies from simulation to real-world environments, providing a robust solution for deploying CAV systems in practical settings.

2 Related Work

In this section, we review the existing literature in this area, highlighting its limitations to establish the motivation for our proposed approach.

Deep Reinforcement Learning in Robotics Training RL or MARL policies in simulation ensures safety and efficiency by mitigating risks to hardware and its surroundings. While imitation learning is commonly used for policy transfer [16, 17], its reliance on real-world data often incurs significant costs. Our approach focuses on simulator-based training to reduce this dependency while maintaining robust real-world performance. Addressing the challenges of sim-to-real transfer, prior studies have introduced techniques such as domain randomization, state normalization, and noise injection to bridge the sim-to-real gap [18, 19, 20]. Building on these advancements, our proposed RSR-RSMARL framework aligns simulator and real-world environments by designing state and action spaces based on hardware capabilities, enabling efficient policy refinement and deployment.

Multi-Agent Systems and CAV Testbeds Existing multi-agent system and CAV vehicular testbeds [9, 3, 10, 11], address diverse research areas such as planning and control, computer vision, collective behavior, autonomous racing, and human-computer interaction. Despite these advancements, most testbeds lack an open-source, detailed framework analysis that integrates communication, RL/MARL, and control with robust safety mechanisms. Our proposed testbed addresses this gap by providing a fully open-source platform that researchers can easily adapt and extend. It features a comprehensive pipeline supporting real-sim-real transfer and integrates CBF-based safety module to ensure safe operation, making it a valuable tool for advancing multi-agent and CAV research.

Safe and Robust RL and MARL Safety has become a critical focus in RL and MARL, particularly for multi-agent systems such as CAVs. Various approaches, including safety shields, barrier functions, and CBF-PID controllers, have been developed to enhance safety by enforcing constraints during decision-making, ensuring collision avoidance and other critical needs [21, 22, 23, 2, 24, 8]. However, real-time constraints must be redefined in multi-agent settings due to inherent communication latency in V2V communication. To address uncertainties, robust RL methods have emerged to improve policy training under uncertain observations, but often overlook explicit safety requirements [15, 14, 25]. The integration of safety and robustness remains a significant challenge, particularly in multi-agent scenarios with delayed observation and agent decision-making. Our work contributes to this field by demonstrating the effectiveness of CBF-based *Safety Shield* that integrates safety constraints directly into the MARL algorithm process, providing a robust framework for safe exploration and control of multi-agent systems under real-world uncertainties.

3 Approach

In this section, we introduce **RSR-RSMARL**, a Real-Sim-Real Robust and Safe Multi-Agent Reinforcement Learning framework that incorporates real-world constraints from the real system into the simulation-based MARL problem formulation and policy training process. RSR-RSMARL consists of three main components. First, we define the state and action spaces and state sharing among agents informed by the real-world hardware system architecture, communication capability and limitations to enable seamless policy transfer. Next, we propose a robust and safe MARL algorithm augmented with a Safety Shield module for safe and efficient training in simulation. Finally, we deploy the trained policies onto real-world hardware, leveraging onboard sensors and V2V communication for evaluation. Figure 1 provides an overview of the RSR-RSMARL architecture.

3.1 MARL Formulation with Real-to-Sim Design

The design of a Robust and Safe MARL problem formulation and policy training algorithm begins with a grounded understanding of real-world conditions and constraints to ensure practical applicability and safety under the simulation-to-reality gap. By aligning the state space, action space, and inter-agent communication with the physical limitations of hardware, the algorithm avoids unrealistic assumptions common in simulated settings. Key real-world factors—such as sensor noise,

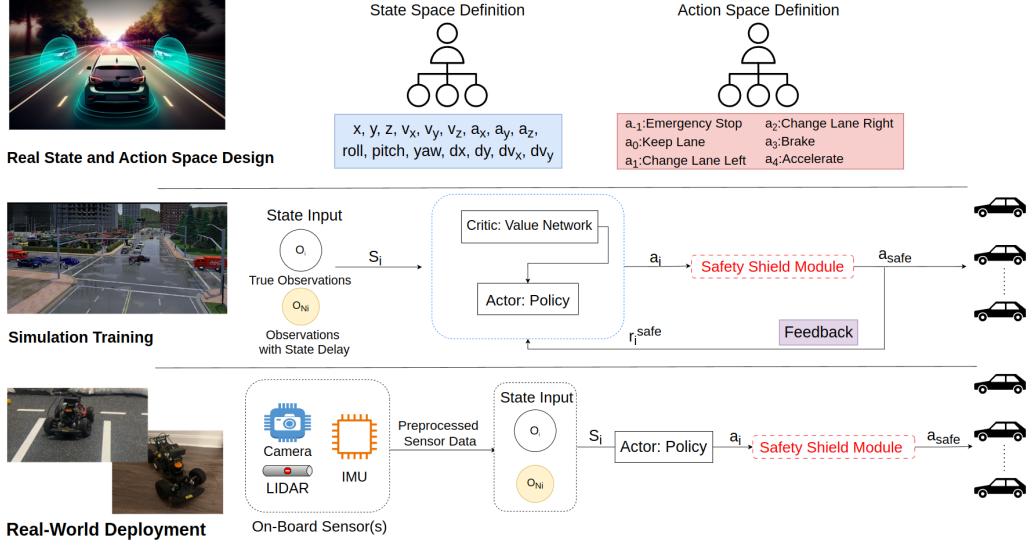


Figure 1: RSR-RSMARL Framework Breakdown. The figure showcases the pipeline of the Real-Sim-Real framework, where an agent interacts with both real-world and simulated environments. In the design phase, state information from real-world sensors (e.g., camera, LiDAR, and IMU) is used to produce state and action spaces, which are then employed in a simulation environment for policy training. The training integrates a value network and actor policy updates, incorporating a Safety Shield Module to ensure safe decision-making. In the deployment phase, the trained policy is transferred back to the real-world system, where high-level actions are processed by a robust control module to generate safe and efficient control outputs.

communication and actuation delays, and environmental obstacles—are explicitly modeled to account for uncertainty and variability [26, 10, 7]. Incorporating these complexities enhances the algorithm’s robustness, enabling it to generalize and adapt effectively to diverse operating conditions while meeting the safety requirements of connected and autonomous vehicles (CAVs).

In particular, in a multi-agent setting, each CAV, referred to as the ego agent i , receives its own observation o_i and a set of shared observations o_{N_i} communicated by neighboring vehicles N_i via vehicle-to-vehicle (V2V) protocols. The shared information includes complementary sensor data and environmental detections, such as obstacle presence and lane boundary features, not directly observable by the ego agent. These measurements are derived from onboard sensors including LiDAR, camera-based lane detection models [27], and others [28]. Additionally, CAVs exchange local state-action histories to mitigate the effects of partial observability and communication delays, enabling more informed action selection. This cooperative approach aims to improve the robustness and safety of decision-making in both simulation and real-world deployments under realistic communication and sensing imperfections.

We formulate a MARL problem based on the state, action, and information sharing through communication among agents as a tuple $G = (S, \mathcal{A}, P, r, \gamma)$, where S is the joint state space of all agents. Each agent i ’s state s_i includes local observation $o_i := \{l_i, v_i, \alpha_i, d_i, c_i\}$. l_i, v_i, α_i are the ego agent’s position, velocity, and acceleration; d_i is processed vision-based features including lane detection results from Ultra Fast Lane Detection (UFLD) [27] and estimated local trajectories; c_i is LiDAR-based collision indicators. \mathcal{A} denotes the discrete action space. When communication is enabled and agent j can share its local observation, $s_{j,i}$ denotes the information sharing between agent j to agent i . The action space a_i of each agent i includes: $a_{i,-1}$: Emergency Stop; $a_{i,0}$: Maintain Lane and Speed; $a_{i,1}$: Change Lane Left; $a_{i,2}$: Change Lane Right; $a_{i,3+k}$: Discrete Braking and Acceleration Actions. The unknown stochastic transition dynamics of the entire system with N agents is defined as $P : S \times \mathcal{A} \times S \rightarrow [0, 1]$. The reward function $r : S \times \mathcal{A} \rightarrow \mathbb{R}$ is given by:

$$r(s, a) = w_1 \|v_i\|_2 - w_2 \|c_i\| + w_3 \|l_i\|, \quad (1)$$

where w_1 , w_2 , and w_3 are weight coefficients for high speed, collision avoidance, and proximity to the goal, respectively. During training and execution, agents use delayed observations $s_{t_{\text{delay}}}$ to account for communication latency. This design ensures policy robustness against transmission delays and varying network reliability, critical for real-world applicability. We aim to train $\pi_\theta(a_i | s_i)$, a decentralized policy parametrized by θ for each agent.

Safety Shield Module: MARL selected actions are checked through a Safety Shield module (Figure 2) [5, 29]. Within the simulation environment, we employ CBF-based constraints for safety validation. We adopt the kinematic bicycle model [30] for vehicles and consider the dynamics \mathbf{x} of a vehicle is affine in terms of its control input \mathbf{u} : $\dot{\mathbf{x}} = f(\mathbf{x}) + g(\mathbf{x})\mathbf{u}$, where \mathbf{x} is defined as $\mathbf{x} := [x, y, \psi, v]$ (x, y are location coordinates, ψ, v are heading angle and velocity). The ego vehicle is subject to speed limit $[v_{\min}, v_{\max}]$ and acceleration limit a_{\min}, a_{\max} . The CBF is the additional safety constraint for the ego vehicle in \mathbf{x}_{ego} , given the target vehicle with the dynamic state \mathbf{x}_{tar} is immediately preceding it, is formulated as (2).

$$h(\mathbf{x}_{\text{ego}}, t | \mathbf{x}_{\text{tar}}) := x_{\text{tar}} - x_{\text{ego}} - cv_{\text{ego}} - \Delta \quad (2)$$

Having \mathbf{u}^{ref} as the reference control provided by the PID (other controllers such as MPC can be applied if available) of an action $a_{i,k} \in \mathcal{A}_i$ to be executed by ego vehicle i , we can utilize the following Quadratic Program (QP) (3) for safety filtering. If the QP is solvable, then $a_{i,k}$ is a safe action for the vehicle.

$$\begin{aligned} \min_{\mathbf{u} \in \mathbb{R}^m} \quad & \frac{1}{2} \|\mathbf{u} - \mathbf{u}^{\text{ref}}\|^2 \quad \text{s.t.} \quad \frac{\partial h(\mathbf{x}, t)}{\partial t} + L_f h(\mathbf{x}, t) + L_g h(\mathbf{x}, t)\mathbf{u} \geq -\gamma h(\mathbf{x}, t) \quad (3) \\ & v_{\min} \leq v_{\text{ego}} \leq v_{\max}, \quad a_{\min} \leq \dot{v}_{\text{ego}} \leq a_{\max} \end{aligned}$$

This modular safety validation ensures that only safe control commands, generated via PID and shielded via CBFs, are executed during policy rollouts.

3.2 Algorithm and Training in Simulation

For our framework’s algorithm, we draw inspiration from the methodologies presented in [5, 2], which provided valuable insights into structuring state and action spaces that are both Safe and Robust for Multi-agent CAVs. This foundation informed the development of Algorithm 1, where careful consideration was given to balancing robustness and computational efficiency. As stated, we adopted logic from [5, 2] to develop our RSR-RSMARL framework. Specifically, [5] proposes a MARL approach that leverages centralized training with decentralized execution (CTDE) to improve coordination among agents in dynamic environments. This method employs shared critic networks during training while enabling independent decision-making during execution, enhancing scalability and real-world applicability.

Building on this foundation, Algorithm 1 adopts the centralized training with decentralized execution (CTDE) paradigm and introduces a key modification: the explicit incorporation of communication-induced delays into the training loop. To model real-world network latency, agents use delayed state information $s_{t_{\text{delay}}}$ drawn from state histories during training. This design enables agents to learn robust decision-making under temporal inconsistencies, better reflecting real-world communication constraints that are often neglected in conventional simulation settings.

3.3 Real-World Deployment

The hardware architecture builds upon the foundational concepts introduced in Section 3.2, while addressing additional challenges such as communication latency. The hardware implementation utilizes Algorithm 1 with the critic component omitted to streamline processing for real-time operation. State inputs are obtained exclusively from onboard sensors, including LiDAR, cameras, and an Inertial Measurement Unit (IMU), to accurately estimate the vehicle’s true state.

The ego vehicle’s observation o_i , together with delayed neighboring vehicles’ observations o_N , is processed and fed into the trained policy. The policy generates an action a_i based on the learned

Algorithm 1: RSR-RSMARL with Delayed Communication Shared States and Safety Shield

```
1 Initialize policy, PPO critic, and Worst-case Q networks  $\theta_i^0, \phi_i^0, \omega_i^0$ ; worst-Q weight  $\lambda_i^0 = 0$ ;  
2 Set maximum delay  $t_{\text{delay}}$  for states to account for communication latency;  
3 for each episode  $E$  do  
4   Initialize  $s = \prod_i s_i \in \mathcal{S}, \mathcal{A} = \prod_i \mathcal{A}_i$ , delayed state buffer  $\mathcal{B} = \emptyset$ ;  
5   Initialize centralized memory  $M = \emptyset$ ;  
6   Rollout( $s, \mathcal{A}$ ): for each step, agent  $i$  do  
7     Update delayed state buffer  $\mathcal{B}$ : store current state  $s_i$  with a delay of  $t_{\text{delay}}$  timesteps;  
8     Retrieve delayed state  $s_i^{\text{delayed}}$  from  $\mathcal{B}$  corresponding to  $t_{\text{delay}}$ ;  
9     Compute safe action set  $\mathcal{A}_i^{\text{safe}} = \text{CBF}(s_i^{\text{delayed}})$  using delayed state  $s_i^{\text{delayed}}$ ;  
10    Choose  $a_i^{\text{safe}} \in \mathcal{A}_i^{\text{safe}}$  based on  $\epsilon$ -greedy if  $\mathcal{A}_i^{\text{safe}} \neq \emptyset$ ; otherwise  $a_i^{\text{safe}} = a_{i,-1}$ ;  
11    Compute agent's control input  $u_i^{\text{safe}} = \text{PID}(s_i^{\text{delayed}}, a_i^{\text{safe}})$  with PID controller;  
12    Execute  $u_i^{\text{safe}}$ , observe next state  $s' = \prod_i s'_i$ , Compute rewards  $r = \{r_i\}$  (1);  
13    Store  $(s_i^{\text{delayed}}, a_i, r_i), \forall i$  in  $M, s \leftarrow s'$ ;  
14  end  
15  Training: for each agent  $i$  do  
16    Compute PPO and worst-Q critic loss gradients  $\nabla_{\phi_i}(\mathcal{L}_i^V), \nabla_{\omega_i}(\mathcal{L}_i^Q)$  [31, 15];  
17    Update  $\phi_i^E \leftarrow \phi_i^{E+1}, \omega_i^E \leftarrow \omega_i^{E+1}$ ;  
18    Compute policy loss gradients  $\nabla_{\theta_i}(\mathcal{L}_i(\theta_i))$ ;  
19    Update  $\theta_i^E \leftarrow \theta_i^{E+1}, \lambda_i^E \leftarrow \lambda_i^{E+1}$ ;  
20  end  
21 end
```

mapping between observed states and control outputs. The action a_i is evaluated by a Safety Shield, which accounts for the vehicle’s physical limitations, environmental uncertainties, and regulatory constraints. If necessary, the Safety Shield modifies the proposed action to produce a safe action a_{safe} , guaranteeing the system operates within feasible and safe bounds. Finally, control inputs are configured based on the vehicle’s dynamic model to optimize performance within the testing environment. This careful alignment between policy design, safety enforcement, and hardware constraints ensures both reliable operation and effective real-world deployment.

4 Experiments and Results

In our experiments, we aim to answer the following questions: (1) Can RSR-RSMARL effectively transfer policies from simulation to the real world by leveraging real-world system states and actions as design constraints, while accounting for uncertainties such as communication delays, sensor noise, and inter-vehicle dynamics? (2) How does RSR-RSMARL’s hybrid control architecture—combining RL policies with traditional controllers and CBFs—compare to alternative baselines in terms of safety and coordination? (3) How critical are robust state and action representations in enabling scalable and generalizable Sim2Real transfer for multi-agent autonomous vehicle systems?

4.1 Real-World Evaluation

We evaluate the proposed framework in real-world environments using two distinct driving scenarios: a 3-lane miniature highway and a 2-lane circular highway. Each environment is tested under three levels of complexity, corresponding to the number of obstacles introduced. Table 1 summarizes the evaluation results, reporting the number of collisions and time to complete each scenario.

On the 3-lane highway, RSR-RSMARL achieves zero collisions across all obstacle variations while maintaining completion times between 34.2 and 36.1 seconds. In contrast, RSR-MARL, which

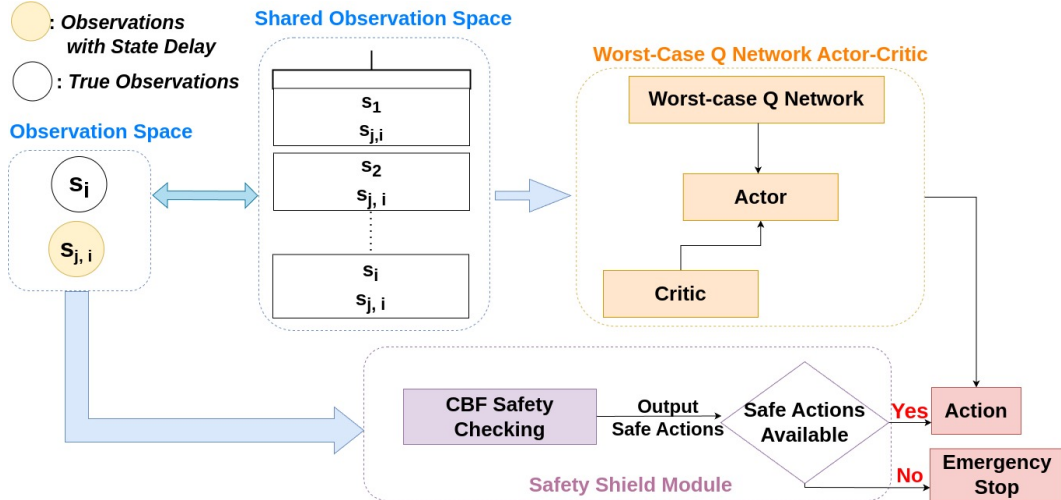


Figure 2: The figure illustrates the hardware policy execution stage pipeline of an agent, with all other agents following the same procedure. During training, both the value network and the worst-Q network contribute to updating the actor’s policy. During testing, Agent i inputs states with uncertainty into its actor, which samples a high-level action a_i . This action is then processed by a robust PID controller to perform path planning and generate a safe control signal u_i .

excludes the Safety Shield module, exhibits a growing number of collisions as the number of obstacles increases. Although RSR-MARL completes each scenario faster, this speed comes at the cost of erratic and risk-prone driving behavior. These findings underscore that faster completion does not equate to a better or safer driving strategy. The deliberate and slightly slower pace of RSR-RSMARL is an intentional trade-off that prioritizes collision avoidance and real-time safety guarantees—hallmarks of a robust and safe system.

Table 1: Evaluation Results on 3-Lane Highway and 2-Lane Oval Highway

Method	Number of Obstacles		
	None	1	2
<i>3-Lane Highway</i>			
RSR-RSMARL	0, 34.2	0, 35.4	0, 36.1
RSR-MARL	1, 31.8	2, 32.5	3, 33.0
No-Comm RSR-RSMARL	0, 36.7	1, 37.9	1, 38.5
<i>2-Lane Oval Highway</i>			
RSR-RSMARL	0, 47.6	0, 48.9	0, 49.7
RSR-MARL	1, 41.3	2, 42.5	3, 43.1
No-Comm RSR-RSMARL	0, 54.8	1, 56.2	1, 57.1

Each entry contains (*number of collisions; time to finish in seconds*).

RSR-RSMARL: Proposed Real-Sim-Real RL with Safety Shield and V2V Communication.

RSR-MARL: Framework variant without Safety Shield module.

No-Comm RSR-RSMARL: RSR-RSMARL variant without V2V Communication.

The No-Comm RSR-RSMARL variant, which disables V2V communication, shows slightly higher completion times and incurs isolated collisions under perturbations. This result highlights the additional robustness provided by inter-agent communication in dynamic environments.

A similar trend is observed in the 2-lane oval highway scenario. RSR-RSMARL again maintains zero collisions, finishing between 47.6 and 49.7 seconds. RSR-MARL’s performance deteriorates

as obstacle complexity increases, and the No-Comm variant—while collision-free in the simplest setting—struggles under more complex conditions.

Overall, these results validate the real-world effectiveness of RSR-RSMARL in achieving safe and efficient autonomous driving under partially observable conditions. The combination of a Safety Shield and V2V communication significantly enhances system robustness and reliability, positioning RSR-RSMARL as the optimal configuration.

4.2 Benchmarking in Simulation

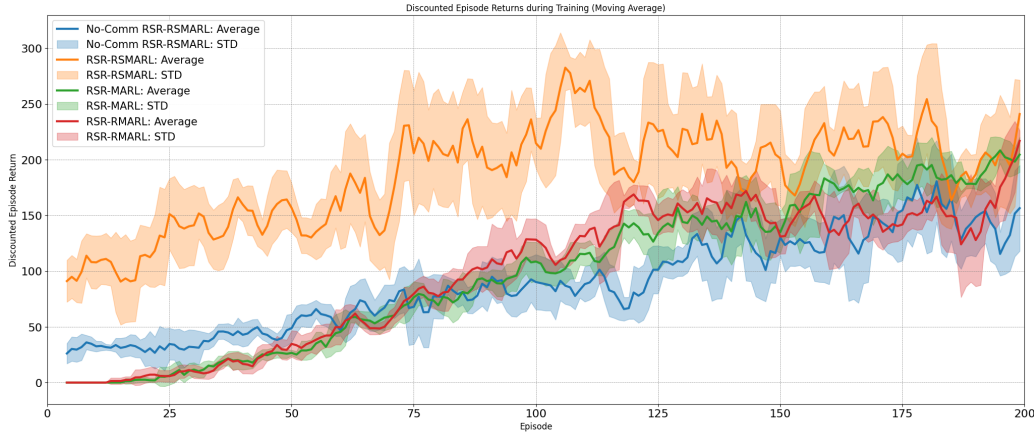


Figure 3: Discounted Efficiency Returns during Training

We benchmarked our method in a simulated highway scenario against several baselines, analyzing the impact of communication delay and CBF removal on collision rate and efficiency return.

The efficiency return shown in Figure 3 captures only the reward from task performance (e.g., speed and goal-reaching). Penalties for safety violations such as collisions are applied separately and detailed in Table 2. This separation helps clarify why some methods may exhibit high efficiency returns despite high collision rates.

Table 2: Evaluation Results

Method	Number of Collisions	Mean Discounted Efficiency Return
Robust MARL	28	60.65
RSR-RSMARL	0	129.52
Non-Robust RSR-MARL	45	25.26
RSR-MARL	42	28.84

Number of Collisions: Total number of collisions recorded over 50 test episodes.

Mean Discounted Efficiency Return: Average cumulative return weighted by completion speed and penalized for collisions.

Robust MARL: Proposed framework with Safety Shield and no communication delay.

RSR-RSMARL: Proposed framework with Safety Shield and V2V Communication.

Non-Robust MARL: Non-Robust Variant without Safety Shield and with communication delay.

RSR-MARL: Variant without Safety Shield module.

Figure 3 shows that RSR-RSMARL achieved the highest efficiency with zero collisions, demonstrating its strength in both safety and performance. Table 2 presents the evaluation results averaged

over 50 testing episodes for each method. As shown in table 2 removing CBFs, even with communication, significantly increases collision risk. While CBF alone reduces collisions, the best results come from combining safety enforcement with reliable communication. This supports the need for both in robust multi-agent autonomy.

5 Limitations

In this paper, we present RSR-RSMARL, a RL framework that incorporates real-world constraints into the Sim-to-Real process, enabling zero-shot deployment on physical hardware. While our framework is well-suited for evaluation on a 1/10th-scale autonomous vehicle testbed, it does have certain limitations. First, we utilize the CARLA simulator as our primary training environment. Although CARLA is a widely adopted and powerful platform for reinforcement learning research, alternative simulation environments may offer closer alignment with specific robotic hardware configurations. This alignment could potentially improve transferability.

Second, our system’s hardware was heavily dependent on onboard sensing and computation, which can become increasingly expensive as additional components are integrated. To reduce long-term costs and improve reusability across various experimental setups, certain external hardware investments—such as a Vicon Motion Capture System—could prove beneficial. This system, for example, can support accurate vehicle lane detection and localization. Moreover, the onboard hardware required significant tuning and configuration effort, which further increased setup complexity.

Finally, though this work focused on RSR MARL with V2V communication, it would be interesting to explore how the proposed framework generalizes to other forms of communication and coordination, such as infrastructure-to-vehicle (I2V) or vehicle-to-cloud (V2C) systems. Investigating these communication paradigms could reveal additional insights into scalability, robustness under variable latency, and the trade-offs between centralized and decentralized decision-making in multi-agent autonomous systems.

References

- [1] U. I. J. P. Office. Saving lives with connectivity: A plan to accelerate v2x deployment non-binding contents, 2024.
- [2] Z. Zhang, S. Han, J. Wang, and F. Miao. Spatial-temporal-aware safe multi-agent reinforcement learning of connected autonomous vehicles in challenging scenarios. pages 5574–5580, 2023.
- [3] N. Hyldmar, Y. He, and A. Prorok. A fleet of miniature cars for experiments in cooperative driving. *Proceedings - IEEE International Conference on Robotics and Automation*, 2019-May:3238–3244, 5 2019. ISSN 10504729. doi:10.1109/ICRA.2019.8794445.
- [4] A. Miller, K. Rim, P. Chopra, P. Kelkar, and M. Likhachev. Cooperative perception and localization for cooperative driving. *Proceedings - IEEE International Conference on Robotics and Automation*, pages 1256–1262, 5 2020. ISSN 10504729. doi:10.1109/ICRA40945.2020.9197463.
- [5] Z. Zhang, H. M. S. Ahmad, E. Sabouni, Y. Sun, F. Huang, W. Li, and F. Miao. Safety guaranteed robust multi-agent reinforcement learning with hierarchical control for connected and automated vehicles. 9 2023. URL <https://arxiv.org/abs/2309.11057v2>.
- [6] S. Han, H. Wang, S. Su, Y. Shi, and F. Miao. Stable and efficient shapley value-based reward reallocation for multi-agent reinforcement learning of autonomous vehicles. *Proceedings - IEEE International Conference on Robotics and Automation*, pages 8765–8771, 3 2022. ISSN 10504729. doi:10.1109/ICRA46639.2022.9811626. URL <https://arxiv.org/abs/2203.06333v2>.
- [7] J. Rios-Torres and A. A. Malikopoulos. A survey on the coordination of connected and automated vehicles at intersections and merging at highway on-ramps. *IEEE Transactions on Intelligent Transportation Systems*, 18:1066–1077, 5 2017. ISSN 15249050. doi:10.1109/TITS.2016.2600504.
- [8] S. Han, S. Zhou, J. Wang, L. Pepin, C. Ding, J. Fu, and F. Miao. A multi-agent reinforcement learning approach for safe and efficient behavior planning of connected autonomous vehicles. *IEEE Transactions on Intelligent Transportation Systems*, 25(5):3654–3670, 2024. doi:10.1109/TITS.2023.3336670.
- [9] A. Mokhtarian, P. Scheffe, M. Kloock, S. Schäfer, Heeseung Bang, Viet-Anh Le, Sangeet Ulhas, J. Betz, S. Wilson, S. Berman, A. Prorok, and B. Alrifaae. A survey on small-scale testbeds for connected and automated vehicles and robot swarms. 2024. doi:10.13140/RG.2.2.16176.74248/1. URL <https://arxiv.org/abs/2408.03539>.
- [10] Y. Shao, M. A. M. Zulkefli, Z. Sun, and P. Huang. Evaluating connected and autonomous vehicles using a hardware-in-the-loop testbed and a living lab. *Transportation Research Part C: Emerging Technologies*, 102:121–135, 5 2019. ISSN 0968-090X. doi:10.1016/J.TRC.2019.03.010.
- [11] C. Tang, B. Abbatematteo, J. Hu, R. Chandra, R. Martín-Martín, and P. Stone. Deep reinforcement learning for robotics: A survey of real-world successes. 8 2024. doi:10.1146/((please)). URL <https://arxiv.org/abs/2408.03539v2>.
- [12] Y. Feng, C. Hong, Y. Niu, S. Liu, Y. Yang, W. Yu, T. Zhang, J. Tan, and D. Zhao. Learning multi-agent loco-manipulation for long-horizon quadrupedal pushing, accepted, ICRA2025. URL <https://arxiv.org/abs/2411.07104>.
- [13] P. Werner, T. Seyde, P. Drews, T. M. Balch, I. Gilitschenski, W. Schwarting, G. Rosman, S. Karaman, and D. Rus. Dynamic multi-team racing: Competitive driving on 1/10-th scale vehicles via learning in simulation. In *7th Annual Conference on Robot Learning*, 2023. URL <https://openreview.net/forum?id=fvXFCHVGn>.

- [14] S. Han, S. Su, S. He, S. Han, H. Yang, and F. Miao. What is the solution for state adversarial multi-agent reinforcement learning? *arXiv preprint arXiv:2212.02705*, 2022.
- [15] Y. Liang, Y. Sun, R. Zheng, and F. Huang. Efficient adversarial training without attacking: Worst-case-aware robust reinforcement learning. *Advances in Neural Information Processing Systems*, 35:22547–22561, 2022.
- [16] M. Torne, A. Simeonov, Z. Li, A. Chan, T. Chen, A. Gupta, and P. Agrawal. Reconciling reality through simulation: A real-to-sim-to-real approach for robust manipulation. 3 2024. URL <https://arxiv.org/abs/2403.03949v1>.
- [17] M. T. Villasevil, A. Jain, V. Macha, J. Yuan, L. L. Ankile, A. Simeonov, P. Agrawal, and A. Gupta. Scaling robot-learning by crowdsourcing simulation environments.
- [18] W. Zhao, J. P. Queralta, and T. Westerlund. Sim-to-real transfer in deep reinforcement learning for robotics: A survey. *2020 IEEE Symposium Series on Computational Intelligence, SSCI 2020*, pages 737–744, 12 2020. doi:10.1109/SSCI47803.2020.9308468.
- [19] Y. Jiang, C. Wang, R. Zhang, J. Wu, and L. Fei-Fei. Transic: Sim-to-real policy transfer by learning from online correction. In *Conference on Robot Learning*, 2024.
- [20] S. S. Sandha, L. Garcia, B. Balaji, F. Anwar, and M. Srivastava. Sim2real transfer for deep reinforcement learning with stochastic state transition delays. In J. Kober, F. Ramos, and C. Tomlin, editors, *Proceedings of the 2020 Conference on Robot Learning*, volume 155 of *Proceedings of Machine Learning Research*, pages 1066–1083. PMLR, 16–18 Nov 2021. URL <https://proceedings.mlr.press/v155/sandha21a.html>.
- [21] L. Brunke, M. Greeff, A. W. Hall, Z. Yuan, S. Zhou, J. Panerati, and A. P. Schoellig. Safe learning in robotics: From learning-based control to safe reinforcement learning. *Annual Review of Control, Robotics, and Autonomous Systems*, 5:411–444, 2022.
- [22] I. ElSayed-Aly, S. Bharadwaj, C. Amato, R. Ehlers, U. Topcu, and L. Feng. Safe multi-agent reinforcement learning via shielding. In *Proceedings of the 20th International Conference on Autonomous Agents and MultiAgent Systems, AAMAS ’21*, page 483–491, Richland, SC, 2021. International Foundation for Autonomous Agents and Multiagent Systems. ISBN 9781450383073.
- [23] Z. Cai, H. Cao, W. Lu, L. Zhang, and H. Xiong. Safe multi-agent reinforcement learning through decentralized multiple control barrier functions, 2021.
- [24] J. Wang, S. Yang, Z. An, S. Han, Z. Zhang, R. Mangharam, M. Ma, and F. Miao. Multi-agent reinforcement learning guided by signal temporal logic specifications. *arXiv preprint arXiv:2306.06808*, 2023.
- [25] S. He, S. Han, S. Su, S. Han, S. Zou, and F. Miao. Robust multi-agent reinforcement learning with state uncertainty. *Transactions on Machine Learning Research*, 2023.
- [26] A. Mokhtarian, P. Scheffe, M. Kloock, S. Schäfer, Heeseung Bang, Viet-Anh Le, Sangeet Ulhas, J. Betz, S. Wilson, S. Berman, A. Prorok, and B. Alrifaae. A survey on small-scale testbeds for connected and automated vehicles and robot swarms. 2024. doi:10.13140/RG.2.2.16176.74248/1. URL <https://rgdoi.net/10.13140/RG.2.2.16176.74248/1>.
- [27] Z. Qin, H. Wang, and X. Li. Ultra fast structure-aware deep lane detection. In *Computer Vision—ECCV 2020: 16th European Conference, Glasgow, UK, August 23–28, 2020, Proceedings, Part XXIV 16*, pages 276–291. Springer, 2020.
- [28] Y. Li, D. Ma, Z. An, Z. Wang, Y. Zhong, S. Chen, and C. Feng. V2x-sim: Multi-agent collaborative perception dataset and benchmark for autonomous driving. *IEEE Robotics and Automation Letters*, 7:10914–10921, 2 2022. ISSN 23773766. doi:10.1109/LRA.2022.3192802. URL <https://arxiv.org/abs/2202.08449v2>.

- [29] H. M. S. Ahmad, E. Sabouni, A. Dickson, W. Xiao, C. G. Cassandras, and W. Li. Secure control of connected and automated vehicles using trust-aware robust event-triggered control barrier functions, 2024. URL <https://arxiv.org/abs/2401.02306>.
- [30] J. Kong, M. Pfeiffer, G. Schildbach, and F. Borrelli. Autonomous driving using model predictive control and a kinematic bicycle vehicle model. In *Intelligent Vehicles Symposium, Seoul, Korea*, 2015.
- [31] J. Schulman, F. Wolski, P. Dhariwal, A. Radford, and O. Klimov. Proximal policy optimization algorithms. *arXiv preprint arXiv:1707.06347*, 2017.

A Appendix

A.1 Modeling and Algorithmic Details

A.1.1 Vehicle Dynamic Model

We adopt a kinematic bicycle model to describe the motion of each F1/10th vehicle. The state of each vehicle is represented as $x = [X, Y, \theta, v]^T$, where X and Y are the position coordinates, θ is the heading angle, and v is the linear speed. The control inputs are the steering angle δ and acceleration a . The continuous-time model is given by:

$$\dot{X} = v \cos(\theta), \quad (4)$$

$$\dot{Y} = v \sin(\theta), \quad (5)$$

$$\dot{\theta} = \frac{v}{L} \tan(\delta), \quad (6)$$

$$\dot{v} = a, \quad (7)$$

where L is the wheelbase of the vehicle.

A.1.2 Simulation vs. Real-World Assumptions

Our simulation environment in CARLA is designed to closely mimic the real-world deployment conditions. We do not assume perfect observability or communication; instead, we explicitly model partial observability and real-time V2V communication delay.

Both the simulation and real-world settings operate under partial observability, where each agent has access to its own local state (e.g., position, heading, velocity) and receives only selected shared information from neighboring vehicles through V2V communication. The communicated states are intentionally limited to reflect bandwidth constraints and to enforce decentralized decision-making.

To account for communication imperfections, our simulator incorporates communication state delay from neighboring vehicles via a specific timestep. These aspects are calibrated to match the communication behavior observed in the real-world hardware platform. This consistent design ensures that policies trained in simulation can generalize to the real world with minimal sim-to-real gap.

A.1.3 Control Barrier Function (CBF) Formulation

To enforce safety during execution, we design a Control Barrier Function $h(x)$ that ensures forward invariance of a safe set $\mathcal{C} = \{x \in \mathbb{R}^n : h(x) \geq 0\}$. Given the vehicle's state x and nominal control u_{nom} , we solve the following Quadratic Program (QP) at each control step:

$$u^* = \arg \min_{u \in \mathbb{R}^m} \|u - u_{\text{nom}}\|^2 \quad (8)$$

$$\text{subject to } \frac{\partial h(x)}{\partial x} f(x) + \frac{\partial h(x)}{\partial x} g(x)u + \alpha(h(x)) \geq 0, \quad (9)$$

where $\alpha(\cdot)$ is an extended class- \mathcal{K} function ensuring asymptotic safety. The resulting control u^* is then applied to the vehicle, overriding the unsafe action when necessary.

CBF Integration into MARL Framework. The MARL policy outputs a nominal control action u_{nom} for each agent based on its observation. This action is passed to the CBF module, which checks for safety violations. If a constraint is active, the CBF-modified control u^* is used instead. The safety filter operates at the same frequency as the policy inference and ensures that no unsafe commands are issued during execution.

A.2 Multi-Agent Reinforcement Learning Setup

We employ a centralized training and decentralized execution (CTDE) framework using the Multi-Agent Proximal Policy Optimization (MAPPO) algorithm. Each agent observes its local state, including position, velocity, and relative distances to nearby vehicles, and communicates high-level

intention data when available. The action space includes continuous throttle and steering commands, while the observation space is composed of ego-state features and LIDAR-based proximity indicators. Communication-aware training includes message dropouts and latency during simulation to better match real-world conditions. Coordination emerges implicitly through shared reward and joint critic training under the CTDE paradigm.

A.3 Neural Network Architecture and Training Parameters

We use the RMAPPO algorithm under the CTDE paradigm. Each agent is equipped with an actor-critic neural network architecture comprising separate networks for the policy (actor) and the value function (critic).

The policy network is a feedforward neural network that maps local observations to continuous action outputs, which include throttle and steering commands. The value network is trained using a shared centralized critic that has access to global information during training. Both networks consist of two hidden layers with ReLU activations, each with 64 and 64 units, respectively. No recurrent (e.g., LSTM or GRU) modules are used in this implementation.

We train policies using a learning rate of 1×10^{-4} for the actor and 2×10^{-4} for the critic. The action space is discretized into 5 levels per control dimension (throttle and steering), resulting in a coarse-grained action output suitable for safety integration and real-world deployment.

Each episode lasts for 400 time steps, and training is conducted over 200 episodes. The number of agents is fixed at three, with agent-specific partial observations. Communication delay is modeled with a fixed delay of one timestep, and each agent communicates only a subset of its state. To align with the reward design described in Appendix A.4, the training incorporates both flow-based and safety-based reward components, with coefficients $\alpha = 3.0$ (flow reward) and $\beta = 0.2$ (average-based cooperation reward). The CBF module is could either be enabled or disabled per experiment.

All training is conducted in a custom CARLA simulation scenario designed to reflect the real-world V2V communication and perception constraints. The training logic is shared between simulation and hardware to minimize the sim-to-real gap.

A.4 Reward Function Design

The reward function design in our MARL framework emphasizes safe, efficient, and goal-directed behavior. Rewards are calculated for each agent individually and then combined with an average reward term to encourage cooperative behavior. The general structure of the reward is:

$$r_i = \alpha \cdot \bar{r}_{\text{team}} + (1 - \alpha) \cdot (r_i^{\text{flow}} + r_i^{\text{dest}}) + r_i^{\text{coll}} + r_i^{\text{safe}} \quad (10)$$

where r_i is the total reward for agent i , \bar{r}_{team} is the team-average reward, and the remaining terms represent individual rewards for velocity tracking (r_i^{flow}), destination progress (r_i^{dest}), collision penalties (r_i^{coll}), and safe action alignment (r_i^{safe}). The weighting parameter $\alpha \in [0, 1]$ balances team cooperation and individual performance.

A.4.1 Simulation Reward Function

During simulation training, the reward components are computed as follows:

- **Velocity Tracking (r_i^{flow}):** Encourages agents to maintain speeds close to a reference target speed ($v_{\text{ref}} = 3.6$ km/h):

$$r_i^{\text{flow}} = 0.2 \cdot \text{flow_coef} \cdot \frac{v_i - v_{\text{ref}}}{3.6}$$

- **Destination Progress** (r^{dest}): Rewards progress along the X-axis from spawn to goal, scaled by a tunable interpolation factor:

$$r_i^{\text{dest}} = \frac{x_i - x_i^{\text{spawn}}}{(x_i^{\text{goal}} - x_i^{\text{spawn}}) \cdot \text{interpolate}}$$

- **Collision Penalty** (r^{coll}): Penalizes collisions based on normalized intensity. Collisions are tracked via a queue and scored proportionally:

$$r_i^{\text{coll}} = - \sum_j \frac{I_{ij}}{40} + 1 \quad (\text{if applicable})$$

- **Safe Action Reward** (r^{safe}): Encourages alignment with true safe action as follows:

$$r_i^{\text{safe}} = \begin{cases} -0.3 & \text{if true action is } -1 \\ 0.1 & \text{if chosen action matches true action} \\ 0 & \text{otherwise} \end{cases}$$

The individual and team-average rewards are combined using a weighted sum controlled by the hyperparameter $\alpha = \text{avg_p}$ (default $\alpha = 1.0$ in most training runs), and the final reward is computed as:

$$r_i = \alpha \cdot (\bar{r}^{\text{flow}} + \bar{r}^{\text{dest}}) + (1 - \alpha) \cdot (r_i^{\text{flow}} + r_i^{\text{dest}}) + r_i^{\text{coll}} + r_i^{\text{safe}} \quad (11)$$

This design allows a balance between decentralized learning and group performance optimization.

A.4.2 Real-World Evaluation Function

In real-world deployment, we retain the same reward structure with a few modifications to properly evaluate our agent’s in the real-world setting.

- **No Ground-Truth Destination:** Due to sensor limitations and safety concerns, we omit r^{dest} in the real world. Destination progress is difficult to quantify precisely as such we remove to avoid discrepancies
- **Collision Approximation via LIDAR:** Instead of using direct collision data from simulation, potential collisions are inferred from minimum LIDAR ranges, and a proximity-based penalty is applied.
- **Simplified Reward Expression:** The real-world reward is simplified to:

$$r_i = \alpha \cdot \bar{r}^{\text{flow}} + (1 - \alpha) \cdot r_i^{\text{flow}} + r_i^{\text{prox}} + r_i^{\text{safe}} \quad (12)$$

where r^{prox} is a negative reward if an obstacle is detected within a critical range threshold (e.g., 0.5 meters).

This reward formulation ensures safe, interpretable, and transferable learning from simulation to hardware, while accounting for limitations in sensory precision and ground-truth availability in real-world deployments.

A.5 Ablation

To assess the robustness of our method, we conducted ablation studies under a domain randomization setup. Specifically, we introduced stochastic noise to all vehicle state observations across all evaluation episodes to simulate discrepancies commonly observed during sim-to-real transfer. This evaluation, referred to as **MARL-DR**, helps isolate the impact of our policy’s robustness when deprived of the structured components of our full framework.

The results of this ablation study are summarized in Table 3. While MARL-DR demonstrates competent performance—outperforming several baseline approaches not shown here—it does not match the safety or efficiency of our complete method. The increased number of collisions and lower mean discounted return underscore the importance of our full pipeline, which includes structured safety mechanisms and communication-aware training.

Table 3: Performance of MARL-DR Under Domain Randomization

Method	Number of Collisions	Mean Discounted Efficiency Return
MARL-DR	10	95.07

Number of Collisions: Total collisions over 50 test episodes.

Mean Discounted Efficiency Return: Cumulative return weighted by completion time and penalized for unsafe behavior.

MARL-DR: MARL policy evaluated with domain-randomized input noise across vehicle states.

A.6 Experimental Results and Visualizations

This section presents additional experimental results and visualizations that complement the findings discussed in the main paper. The figures below highlight both quantitative trends and qualitative behaviors observed during training and deployment in the CARLA simulator, as well as on the physical vehicle platform.

A.6.1 CARLA Simulation Snapshots

We include selected frames from CARLA simulation runs that depict both successful and failed navigation scenarios. These images are useful for visually understanding how the trained policy behaves in complex multi-agent environments.

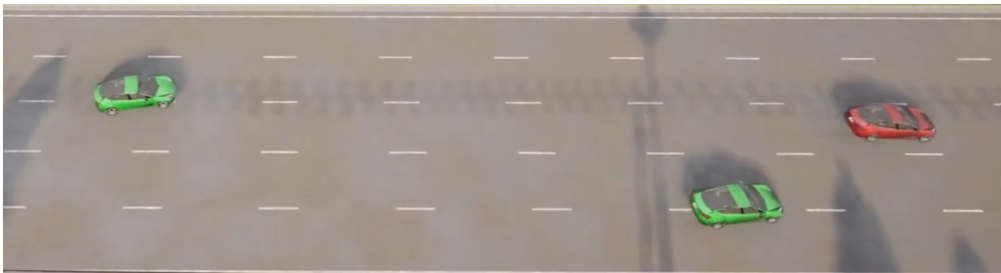


Figure 4: CARLA Simulation: Successful Merging and Lane Change

A.6.2 Real-World Deployment Snapshots

Below we present real-world screenshots and camera captures from the demonstration video, illustrating policy performance on the physical F1/10th vehicle. These include clear cases of safe navigation as well as edge-case behaviors.

We would like to emphasize that the road map setting in CARLA is not exactly the same as our lab testing environment, our trained RSMARL policy still has the best performance compared with baselines as shown in the experiment results in Table 1. This validates the robustness of our proposed method and its zero-shot transfer property even with Sim2Real gap.

A.7 Communication Infrastructure and Safety Interventions

This section provides details on the V2V communication infrastructure deployed during real-world testing, as well as the integration and impact of the safety intervention module.



Figure 5: CARLA Simulation: Failure Case with Rear-End Collision

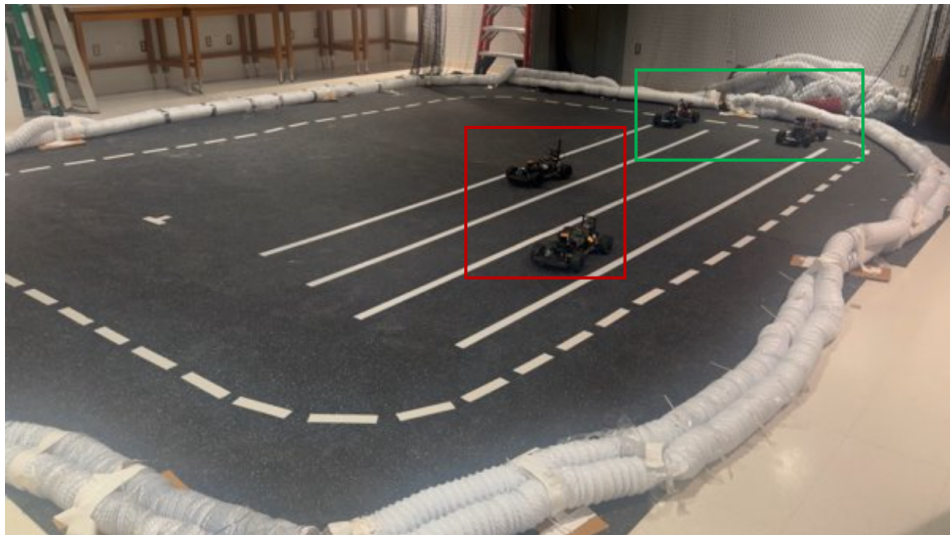


Figure 6: Real-World Environment Setting

A.7.1 Communication Framework: Hardware and Software

Each vehicle in the fleet was equipped with an onboard Jetson Orin Nano (8GB) running ROS1 Noetic on Ubuntu 20.04. For real-world deployment, we rely on a communication infrastructure built upon the Robot Operating System (ROS 1). ROS provides a publish-subscribe messaging architecture that enables real-time data exchange between distributed components - perception modules, control policies, and safety monitors.

To support multi-agent systems and inter-vehicle communications, the deployment architecture integrates DDS-like behavior via ROS topics, where each agent publishes its state (pose, velocity, intent) and subscribes to the state of other agents. Although ROS 1 does not natively use DDS as its trans-

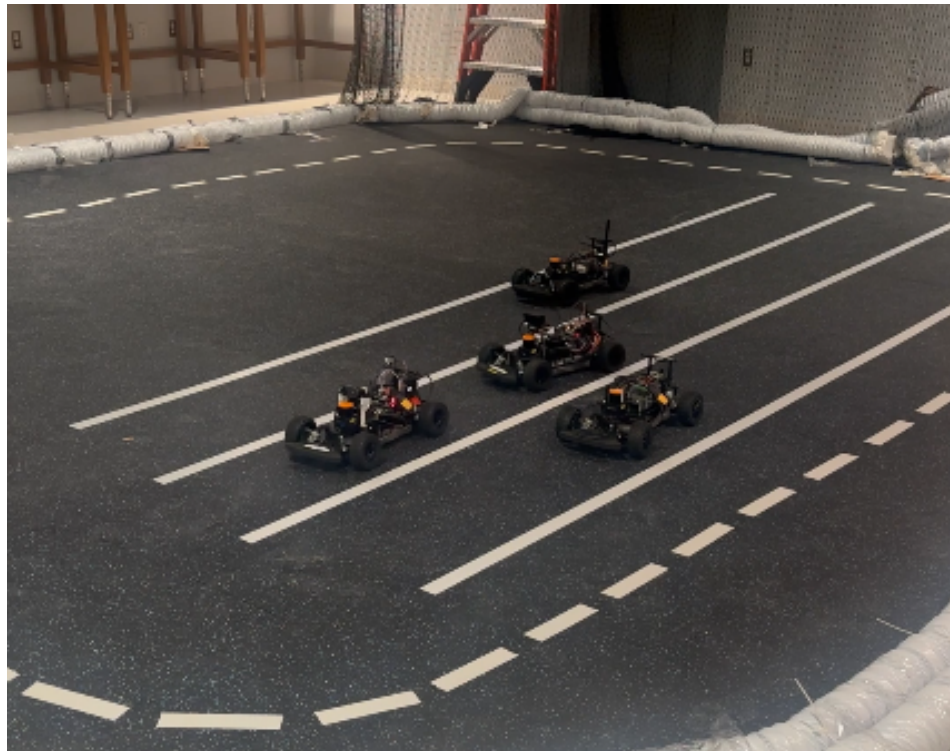


Figure 7: Real-World Test: Lane Following and Obstacle Avoidance



Figure 8: Real-World Test: Drift Caused by Abrupt Control Perturbation

port layer (unlike ROS 2), we emulate similar behavior by establishing time-stamped, namespaced topics and synchronized subscribers to achieve low-latency, best-effort communication.

The software communication module was built using a lightweight UDP protocol implemented in Python. Each agent broadcast its local state – including position, velocity, orientation, and intended action – at a frequency of 10 Hz.

A.7.2 Observed Communication Delays and Losses

To simulate communication imperfections such as latency or packet delay, we inject artificial time shifts in message callbacks (up to 0.3 seconds), mirroring real V2V communication effects. This ensures that the deployed system remains robust even in network-constrained environments.

A.7.3 Safety Interventions via Control Barrier Functions (CBFs)

To ensure real-time safety, a CBF-based module was integrated into the control stack of each vehicle. The CBF evaluated the safety of each proposed action before execution and made real-time corrections to prevent imminent collisions or boundary violations.

Across all real-world trials, the CBF intervened in approximately 14.2% of executed steps. Most interventions occurred in the following scenarios:

- High-speed approach with delayed V2V updates.
- Sudden deceleration of a leading vehicle not yet reflected in received packets.
- Mismatched lane predictions due to drift or occlusion.

A.7.4 Impact of Communication on Safety and Coordination

The presence of V2V communication significantly improved cooperative behavior among agents, especially in scenarios involving lane merging and intersection negotiation. Figure 9 compares the frequency of safety violations and CBF activations between communication-enabled and communication-disabled deployments.

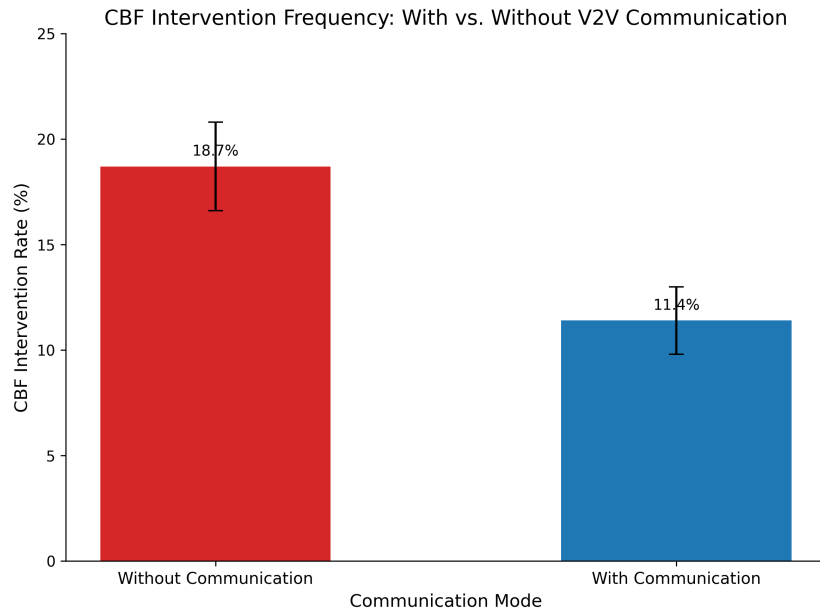


Figure 9: CBF Intervention Frequency: With vs. Without V2V Communication

The data indicates that shared information reduces both the need for reactive overrides and the likelihood of unsafe maneuvers. Furthermore, the coordination enabled by V2V helped stabilize policy outputs during high-density interactions, reducing the average intervention rate from 18.7% (no communication) to 11.4% (with communication).